Received: 3 June 2022 | Revised: 27 July 2022 | Accepted: 27 July 2022

DOI: 10.1002/jcc.26981

RESEARCH ARTICLE

Journal of COMPUTATIONAL CHEMISTRY WILEY

Investigation of glucose electrooxidation mechanism over N-modified metal-doped graphene electrode by density functional theory approach

Derya Düzenli[1,2] | Isik Onal[3] | Ilker Tezsevin[4]

[1]General Directorate of Mineral Research and Exploration, Ankara, Turkey

[2]Turkish Energy, Nuclear and Mineral Research Agency, Rare Earth Elements Research Institute, Ankara, Turkey

[3]Faculty of Engineering, Department of Chemical Engineering, Middle East Technical University, Ankara, Turkey

[4]Department of Applied Physics, Eindhoven University of Technology, Eindhoven, The Netherlands

Correspondence
Ilker Tezsevin, Department of Applied Physics, Eindhoven University of Technology, P.O. Box 513, 5600 MB Eindhoven, The Netherlands.
Email: i.tezsevin@tue.nl

Abstract

In this work, various precious and non-precious metals reported in the literature as the most effective catalysts for glucose electrooxidation reaction were investigated by the density functional theory (DFT) approach in order to reveal the mechanisms taking place over the catalysts in the fuel cell. The use of a single-atom catalyst model was adopted by insertion of one Au, Cu, Ni, Pd, Pt, and Zn metal atom on the pyridinic N atoms doped graphene surface (NG). β form of D-glucose in alkaline solution was used to determine the reaction mechanism and intermediates that formed during the reaction. DFT results showed that the desired glucono-lactone was formed on the Cu-3NG electrode in a single-step reaction pathway whereas it was produced via different two-step pathways on the Au and Pt-3NG electrodes. Although the interaction of glucose with Ni, Pd, and Zn-doped surfaces resulted in the deprotonation of the molecule, lactone product formation did not occur on these electrode surfaces. When the calculation results are evaluated in terms of energy content and product formation, it can be concluded that Cu, Pt, and especially Au doped graphene catalysts are effective for direct glucose oxidation in fuel cells reactor.

KEYWORDS
DFT, electrooxidation, glucose, single atom catalyst

1 | INTRODUCTION

Diminishing of natural energy resources due to high global energy demand and increasing environmental awareness entails the development and use of clean energy sources. Therefore, research efforts aimed at diversifying clean energy sources, and boosting their efficiency and sustainability have been accelerated. Among various clean energy sources, fuel cells (FCs), which enable direct conversion of chemical energy to electrical energy with the most efficient, clean, and versatile ways, have found many application areas such as in transport and space projects.[1–4] FCs are generally classified according to the type of fuel and electrolyte materials they utilize.[4] Likewise, the working conditions and desired performances of FCs determine their usage area. Although one of the most popular FCs is the hydrogen-fed polymer electrolyte membrane fuel cells (PEMFCs), the difficulties of the storage and transportation of the H_2 gas lead to the search for different fuel resources as alternatives.[5–8] As an alternative to PEMFCs, the direct liquid fuel cells (DLFCs) provide an opportunity to use various types of fuels ranging from alcohols, such as methanol, ethanol, or propanol,[9–12] to non-alcohol materials including formic acid and alkaline formate salts,[9,13,14] hydrazine,[15–17] glucose,[5,6,18–23] and borohydride.[24–26] Hence, DLFCs is one of the most promising candidates for FC application areas with enhanced safety handling of these liquid fuels.

Glucose ($C_6H_{12}O_6$), one of the main energy sources of all living organisms and mainly produced via photosynthesis, is the most abundant monosaccharide available in nature. The principle of fast and reliable determination of the amount of glucose in the blood, and energy production directly from glucose are very similar to each other.[19] Electrooxidation of glucose is an essential process required both for the fast and reliable detection of glucose levels in the blood of diabetes patients via a sensor and for glucose use as a DLFC fuel candidate to achieve clean and sustainable energy goals.[27,28] In addition to these, the conversion of glucose to other derivatives such as gluconic, carboxylic, and glucaric acid via electrocatalytic oxidation reaction has been also applied to produce valuable chemical compounds for use in industry.[23] Direct electrooxidation of non-toxic, non-flammable, and non-volatile glucose is performed using enzymatic, microbial, and non-enzymatic FC techniques. Among these, the non-enzymatic FCs have been the subject of more research because of the difficulties encountered in the other two methods that pose major obstacles to their commercial use and dissemination of direct glucose FCs (DGFC).[29,30]

Although several studies were done on the glucose electrooxidation reaction (GOR) and the theories have been presented, the mechanism is still not fully understood. Theoretically, in the case of complete glucose oxidation, a high energy density can be achieved along with 24 electrons released which is hard to achieve in practice.[30–33] The products after complete oxidation of glucose have been identified by chromatographic and spectroscopic techniques as aliphatic gluconic acid ($C_6H_{12}O_7$) and aromatic gluconolactone ($C_6H_{10}O_6$) which further hydrolyses to gluconic acid spontaneously.[34–36] Two electrons are released in the anode for each glucose molecule as shown in the following reaction steps[33,34]:

$$\text{Anode}: C_6H_{12}O_6 + OH^- \rightarrow C_6H_{10}O_7 + H_2O + 2e^-$$

$$\text{Cathode}: 0.5O_2 + H_2O + 2e^- \rightarrow 2OH^-$$

$$\text{Overall reaction}: C_6H_{12}O_6 + 0.5O_2 \rightarrow C_6H_{12}O_7$$

In order to achieve high performance and complete oxidation, platinum-based catalysts are widely used in electrooxidation reactions both in non-enzymatic FC and sensor applications due to their good activity, electrical properties, and corrosion resistance despite their high cost.[37–39] When the performance of the Pt catalysts was compared in different environments, it was seen that alkaline electrolyte activates the direct electrooxidation of fuels better than the acidic and neutral electrolytes. This situation has been attributed to the faster kinetics of the cathode oxygen reduction reaction (ORR) and the anode fuel oxidation reaction in alkaline FCs.[13,22,29,40,41] It is stated that the improvement of the kinetics of the reactions taking place at the anode and cathode (ORR) allows the use of non-precious metal catalyst instead of Pt or the reduction of Pt amount by alloying. Also, the performance degradation of the Pt-electrode as a result of the chemisorption of carbonated intermediates can be avoided in these ways.[42] PtPd and PdPtAu,[20] Pd_xRh/C,[21] Au/Ni foam,[22] Fe-Ni-Co/C,[30] PtRu/C,[31] Pd/C,[32] Pd_3Cu-B/C,[43] Co_xFe_y/graphitic tube[44] can be named as some of the examples of Pt-alloy and non-precious catalytic systems for DGFCs.

Another way to mitigate the amount of precious metal is the use of single-atom catalysts (SAC) supported on carbon or metal-based support materials that have experimentally proven to be efficient in various conversion processes such as hydrogen evaluation reaction, ORR, and many other (electrochemical) oxidation/reduction reactions.[45–52] The major challenge in the SAC system is to maintain the durability of the catalytic structure while increasing its chemical activity. Doping of catalysts, especially on carbon-based materials, with additive atoms like nitrogen or boron, is suggested as a solution to stabilize the loaded metal by increasing its bonding energy with the surface.[53–59] Cheng et al. experimentally demonstrated that Pt metal can be loaded on nitrogen-doped graphene (3NG) surface in desired sizes ranging from a single atom to a small cluster without agglomeration by regulating the metal deposition cycle with the atomic layer deposition method.[46] Among various configurations, pyridinic incorporation of nitrogen into graphene is reported as the most active type for the ORR reaction in electro-catalytic applications.[60,61] Also, we reported theoretically and experimentally that N-doping into the graphene improves the catalytic performance of the Pd-electrode for glucose electrooxidation in an alkaline medium in the previous work.[6]

In the light of this knowledge, the interactions of the glucose molecule with single metal atoms that are used widely in GORs, including precious (Au, Pt, Pd) and non-precious (Ni, Cu, and Zn) atoms, anchored on pyridinic-nitrogen decorated graphene substrates (3NG) were studied in water medium as a solvent via density functional theory (DFT) calculations in this work. The main purpose of the study is to determine the most active metal for the oxidation of glucose and investigate the mechanism through the intermediates that formed during the reaction.

2 | COMPUTATIONAL METHODS

The same surface model and computational strategy explained in our previous work[6] were also employed for the calculations reported in this study. All DFT calculations reported in this work were carried out utilizing the B3LYP[62–64] method provided in Gaussian 09[65] software. Parallel to our previous work, LANL2DZ effective core pseudopotentials were utilized for transition metal atoms (Pd, Pt, Au, Cu, Ni, Zn) whereas 6-31G (d,p) basis set was employed for non-metal atoms (C, H, N). The convergence criteria involving gradients were reported as 0.000450 hartree/bohr for maximum force, 0.000300 hartree/radian for root-mean-square (rms) force, 0.001800 bohr for maximum displacement, and 0.001200 radian for rms displacement in Gaussian software. In addition to previous settings, all calculations considered here were performed under forcefields simulating a solvent environment. In order to perform the calculation in the presence of a solvent, settings for the predefined properties for water as solvent was used. The vibrational frequency analysis was also carried out to ensure the stability of the studied geometries and to find the vibrational

frequencies of the system. The scaling factor was taken as 0.96 for the B3LYP method to reproduce experimental fundamentals recommended in the literature.[66]

The binding energies of the glucose ($C_6H_{12}O_6$), water (H_2O), and hydroxyl (OH) species on the nitrogen-decorated single metal-doped graphene (M-3NG) (M = Au, Pt, Pd, Ni, Cu, and Zn) surface were calculated by using Equation (1) for the zero-point corrected energy values.

$$\Delta E_B = E_{M-3NG+adsorbate} - (E_{M-3NG} + E_{adsorbate}) \quad (1)$$

here, $E_{M-3NG+adsorbate}$ was the energy of the catalyst with adsorbed species. $E_{Glucose}$, E_{OH}, $E_{adsorbate}$ were the energies of single species, and E_{M-3NG} was the energy of the clean M-3NG surface. In these calculations, all energies were calculated under solvent (water) conditions.

In addition to the energetic calculations, a full population analysis was also performed to obtain the localization of the highest occupied molecular orbital (HOMO) and the lowest unoccupied molecular orbital (LUMO) over the catalytic systems considered. Equations (2-6) were used to process population data to get chemical hardness, chemical potential, electronegativity, electrophilicity, and HOMO-LUMO gap of the M-3NG systems before and after interacting with the hydroxyl and glucose species.

$$\text{Chemical hardness}\,(\eta) = \frac{I-A}{2} \quad (2)$$

$$\text{Chemical potential}\,(\mu) = -\frac{I+A}{2} \quad (3)$$

$$\text{Electronegativity}\,(\lambda) = -\mu \quad (4)$$

$$\text{Electrophilicity}\,(\omega) = \frac{\mu^2}{2\eta} \quad (5)$$

$$E_{gap} = E_{HOMO} - E_{LUMO} \quad (6)$$

here, I is equal to the minus value of HOMO energy and A is the minus value of LUMO energy.[67,68]

3 | RESULTS AND DISCUSSION

In our study, a single metal atom catalyst anchored on the nitrogen decorated graphene system (M-3NG) was used to examine the electrooxidation reaction tendency of a glucose molecule with various metal-doped surfaces. Also, the first and second steps of the oxidation reaction mechanism were investigated by DFT approach. The first step is C—H or C—O—H bond activation of the glucose. It is accepted as the rate-determining step for many hydrocarbon oxidation reactions,[69] and the second step is considered to be the oxidation of the activated glucose as stated in the literature.[33,35,70,71] The open form of glucose structure was used to reveal the oxidation mechanism of the $C_6H_{12}O_6$ with the supported/unsupported Au clusters in the theoretical studies.[70,71] In the mechanism proposed by Ishimoto et al., an aliphatic glucose was first attached to the OH species adsorbed on the surface, then water was formed by detaching the H from the CHO group by the OH species in solution, and finally, gluconic acid ($C_6H_{12}O_7$) was formed by the transfer of the surface OH-species to the deprotonated oxygen.[71] Gluconic acid has been reported as the product of GOR at the anode by releasing two electrons in the FC.[22,34] Here, we used the cyclic form of D-glucose, which is defined as a thermodynamically stable structure.[35,36,72] Between the α and β forms of D-glucose, the more stable β form[36] was chosen for electrooxidation reaction calculations. In the case of the cyclic form, it has been reported that first glucono-lactone ($C_6H_{10}O_6$) is formed as an intermediate, and then it is followed by hydrolysis to gluconic acid either spontaneously or catalytically.[33,35,73] The GOR mechanisms through the formation of glucono-lactone mechanisms were therefore examined by DFT method during the study.

To observe the catalytic effect on the oxidation of $C_6H_{12}O_6$ to $C_6H_{10}O_6$ a SAC model structure was prepared by anchoring a metal atom on a graphene surface decorated with pyridinic N atoms (as shown in Figure 1A-D). Here, a metal atom was placed in the surface vacancy positioned at the center of three N-atoms as shown in Figure 1C. Insertion of the metal atom into the N-doped surface does not cause perturbation on the substrate surface; however, the distance between metal atoms and N-atoms showed a difference for each system as shown in Table 1 due to positioning of the metal out of plane. While the longest M—N distances belong to Au-3NG system (2.68, 2.68, and 2.72 Å), M—N bond distance is the shortest for Ni-3NG catalyst (1.91, 1.91, and 1.93 Å). The degree of the perturbation of the graphene surface after the insertion of metal atom has been attributed to the number of the electron shells in the metal atoms.[74] Among the metal atoms investigated in our system, Au metal has the highest atom number so the M—N distance is the longest. Conversely, Ni atom has the shortest M—N distance with the smallest atom number. These results are compatible with the literature.

Before studying the interaction of electrode surfaces with the molecules present in the electrolyte, some electronic and structural properties of the M-3NG systems such as chemical hardness, chemical potential, electronegativity, and electrophilicity were calculated from the highest occupied molecular orbital (HOMO) and lowest unoccupied molecular orbital (LUMO) value and reported in Table 2. Among all the electrode surfaces, the highest LUMO value was calculated for Au-3NG (3.77 eV) electrode system. LUMO values of the other surfaces were very close to each other and varied in the range of 2.31–2.42 eV. Likewise, chemical potential and electrophilicity values, which are interpreted as the tendency of the reaction, showed the same trend. As seen in Table 2, the electrophilicity value for Au-3NG is significantly higher (37.72 eV) and the HOMO-LUMO band gap is the smallest. Therefore, the activity of the Au-3NG surface can be expected to be higher than the other surfaces. Based on our Mulliken charge analysis, the Au-3NG system appeared to behave differently from the other systems considered. Instead of donating electrons to

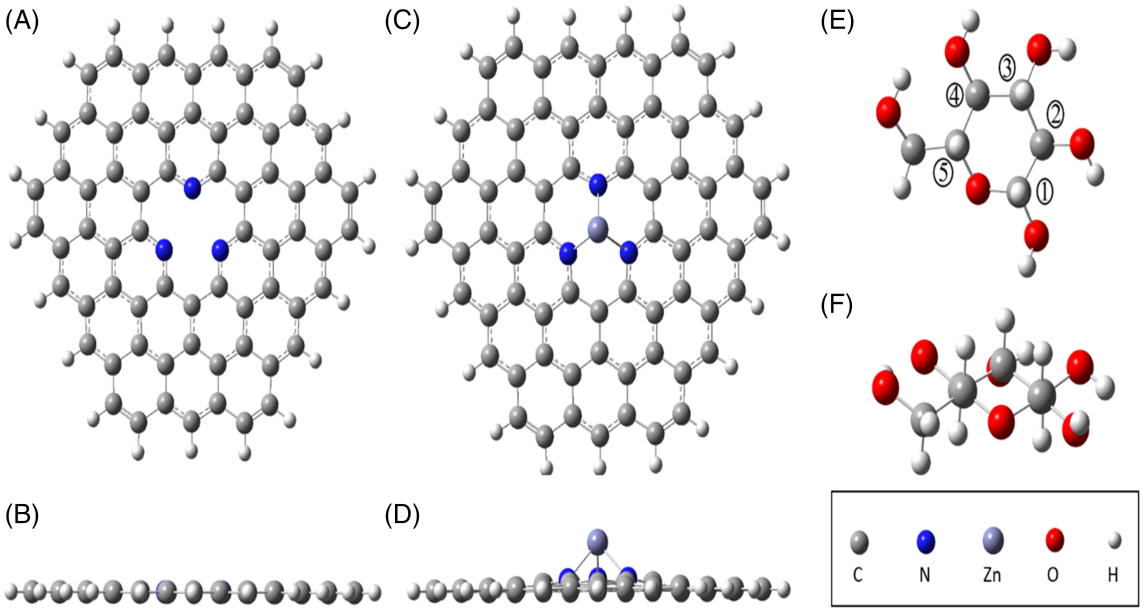

FIGURE 1 Top and side views of (A and B) N decorated graphene (3NG), (C and D) Zn anchored on 3NG, and (E and F) glucose in water (①–⑤ represent considered reaction sites for the interaction with OH radicals in electrolyte) (please refer to the Data S1 xyz data file for better visualization of the outputs)

M—N bond length	Au-3NG	Pt-3NG	Pd-3NG	Ni-3NG	Cu-3NG	Zn-3NG
M—N1 (Å)	2.68	2.14	2.19	1.91	2.05	2.05
M—N2 (Å)	2.68	2.14	2.19	1.91	2.05	2.05
M—N3 (Å)	2.72	2.57	2.47	1.93	2.05	2.05

TABLE 1 Metal-nitrogen bond length distribution over the single-atom catalysts considered

Property	Au-3NG	Pt-3NG	Pd-3NG	Ni-3NG	Cu-3NG	Zn-3NG
HOMO (eV)	4.19	4.25	4.24	4.21	4.32	3.90
LUMO (eV)	3.77	2.37	2.35	2.32	2.42	2.31
Chemical hardness (eV)	0.21	0.94	0.95	0.94	0.95	0.80
Chemical potential (eV)	−3.98	−3.31	−3.30	−3.27	−3.37	−3.11
Electronegativity (eV)	3.98	3.31	3.30	3.27	3.37	3.11
Electrophilicity (eV)	37.72	5.83	5.74	5.65	5.97	6.05
HOMO-LUMO gap (eV)	0.42	1.88	1.89	1.89	1.90	1.59
Mulliken charge on metal	−0.42	+0.38	+0.38	+0.95	+0.39	+1.36

TABLE 2 DFT calculated properties of single atom catalysts considered

Abbreviations: DFT, density functional theory; HOMO, highest occupied molecular orbital; LUMO, lowest unoccupied molecular orbital.

the substrate surface (as in the other M-3NG catalysts considered), Au anchored on 3NG accepted electrons from the substrate resulting in a negative charge.

As the next step, the adsorption of individual H_2O, OH, and $C_6H_{12}O_6$ molecules on M-3NG systems have been studied. Thus, the effect of the surface electronic structure on the adsorbent-adsorbate interaction force can be seen clearly. Different orientations of $C_6H_{12}O_6$ molecule were considered to investigate the behavior of all five-reaction sites shown in Figure 1E and the result for energetically most favorable interaction was reported. According to the DFT calculations in the solution phase using water as the solvent, the binding of all three species was found to be the strongest on Au-3NG catalyst that are compatible with the smallest HOMO-LUMO energy band gap and highest electrophilicity value, as reported in Tables 2 and 3. In terms of glucose adsorption, when the $C_6H_{12}O_6$ was approached by the CH_2—OH group located outside the ring, it adsorbed more strongly for all surfaces within the different binding orientations considered for it. Oxygen molecule attached to Au metal with an adsorption energy of −0.96 eV at a distance of 2.16 Å. In the case of H atoms directly bonded to the C atom, the $C_6H_{12}O_6$

TABLE 3 Adsorption energies of molecules on M-NG catalyst

Adsorption energy (eV)	Au-3NG	Pt-3NG	Pd-3NG	Ni-3NG	Cu-3NG	Zn-3NG
Glucose	−0.96	−0.39	−0.30	−0.38	−0.60	−0.32
H_2O	−1.11	−0.70	−0.55	−0.67	−0.89	−0.61
OH	−3.39	−3.26	−2.08	−3.07	−2.49	−3.08

TABLE 4 Glucose binding energies on hydroxylated M-3NG surfaces and binding energy of adsorption glucose

Property	Au-3NG	Pt-3NG	Pd-3NG	Ni-3NG	Cu-3NG	Zn-3NG
Glucose binding energy (eV)	−0.30	−0.37	−0.65	−0.30	−0.49	−0.32
Surface properties						
HOMO (eV)	4.75	4.10	4.27	4.77	4.25	4.35
LUMO (eV)	3.76	2.68	3.78	3.41	3.74	2.52
Chemical hardness (eV)	0.49	0.71	0.25	0.68	0.26	0.91
Chemical potential (eV)	−4.26	−3.39	−4.02	−4.09	−4.00	−3.44
Electronegativity (eV)	4.26	3.39	4.02	4.09	4.00	3.44
Electrophilicity (eV)	18.34	8.09	32.97	12.34	31.27	6.45
HOMO-LUMO gap (eV)	0.99	1.42	0.49	1.36	0.51	1.83
Mulliken charge on metal	−0.03	+0.57	+0.01	+0.59	+0.06	+0.99
Mulliken charge on OH ads.	−0.41	−0.40	−0.46	−0.47	−0.49	−0.53

Abbreviations: HOMO, highest occupied molecular orbital; LUMO, lowest unoccupied molecular orbital.

molecule rotated and approached the Au metal with an oxygen atom of the ring at a distance of 2.23 Å. The energy release for this orientation was −0.73 eV. On the other hand, alcoholic OH groups and OH group attached to the hemiacetal carbon of $C_6H_{12}O_6$ bonded to the surfaces with −0.78 and −0.64 eV respectively. The glucose adsorption energy over Au-3NG surface was found approximately three times greater than on Pt, Pd, Ni, and Zn and nearly two times greater than on Cu surfaces (Table 3). Among the three species considered, H_2O, OH, and $C_6H_{12}O_6$, OH binding was found to be the most favorable process on all surfaces with an absolute binding energy of at least 2.08 eV. Therefore, OH-adsorbed M-3NG surfaces were used in the investigation of the glucose oxidation as described in the incipient hydroxyl oxide adatom model (IHOAM).[27,75]

When the adsorption energies of all molecules on the Pd-NG surface are compared with the values obtained on the solution-free surface reported in the previous work,[6] the effect of water as a solvent can be seen clearly. For the solution-free catalytic system, the individual interaction of $C_6H_{12}O_6$ (−0.64 eV, now −0.30 eV), H_2O (−0.81 eV, now −0.55 eV), and OH (−3.24 eV, now −2.08 eV) molecules were seen to be energetically stronger than that of the solution-added system. The presence of the water around the electrode weakened the interaction of molecules with the surface thermodynamically as expected but did not impede.

Since the interaction of the adsorbate species with the surface changes the electronic properties of the system, the properties of the OH-adsorbed surfaces were re-evaluated over the new electronic energy values as shown in Table 4. Therefore, it would be more accurate to consider the OH-adsorbed surface as a new system and evaluate it among themselves. The OH molecule was adsorbed at the top of the single metal in a tilted position for all systems and the most feasible energy values belong to Pd and Cu-doped surfaces. As seen in Table 4, covering the surface with an OH molecule increased the electrophilicity value of both Pd and Cu-doped surfaces dramatically while quenching this value for Au-doped surface. Moreover, the electrophilicity value of the Zn-doped surface remained constant and a slight increase was observed for the Pt and Ni-doped surfaces. In addition, the lowest band gap value again belongs to both Pd and Cu-surfaces as seen in Table 4. In the second step, we placed the $C_6H_{12}O_6$ molecule next to the strongly adsorbed OH molecule over surfaces in different orientations since this is defined as the first step of $C_6H_{12}O_6$ electrooxidation reaction. The interaction of the $C_6H_{12}O_6$ molecule with the OH species adsorbed on Pd-3NG surface was strongest as expected (−0.65 eV) as seen in Table 4. In this case, $C_6H_{12}O_6$ molecule made a bond through the OH group attached to the hemiacetal C atom of the ring. After the interaction, the distance between O—H bond of $C_6H_{12}O_6$ molecule extended from 0.97 to 1.02 Å, which looked to be completely separated from the ring as seen in Figure 2A. The distance between the surface OH molecule and the H atom of the ring was calculated as 1.54 Å. While the O and hemiacetal C bond length shrank from 1.39 to 1.37 Å, the H atom attached to the hemiacetal C slightly moved away from 1.10 to 1.11 Å as seen in Figure 2A. The other side of the $C_6H_{12}O_6$ molecule again has a weaker bond such as the CH_2—OH group (−0.16 eV). The CH_2—OH group located outside the ring is an active site for the clean metal-doped surface, while the reactive site is hemiacetal OH site for the OH-adsorbed electrolyte surface. This can be explained by the fact that the hemiacetalic OH group is more acidic than that of the alcoholic OH group.[76] So the interaction between surface OH and this

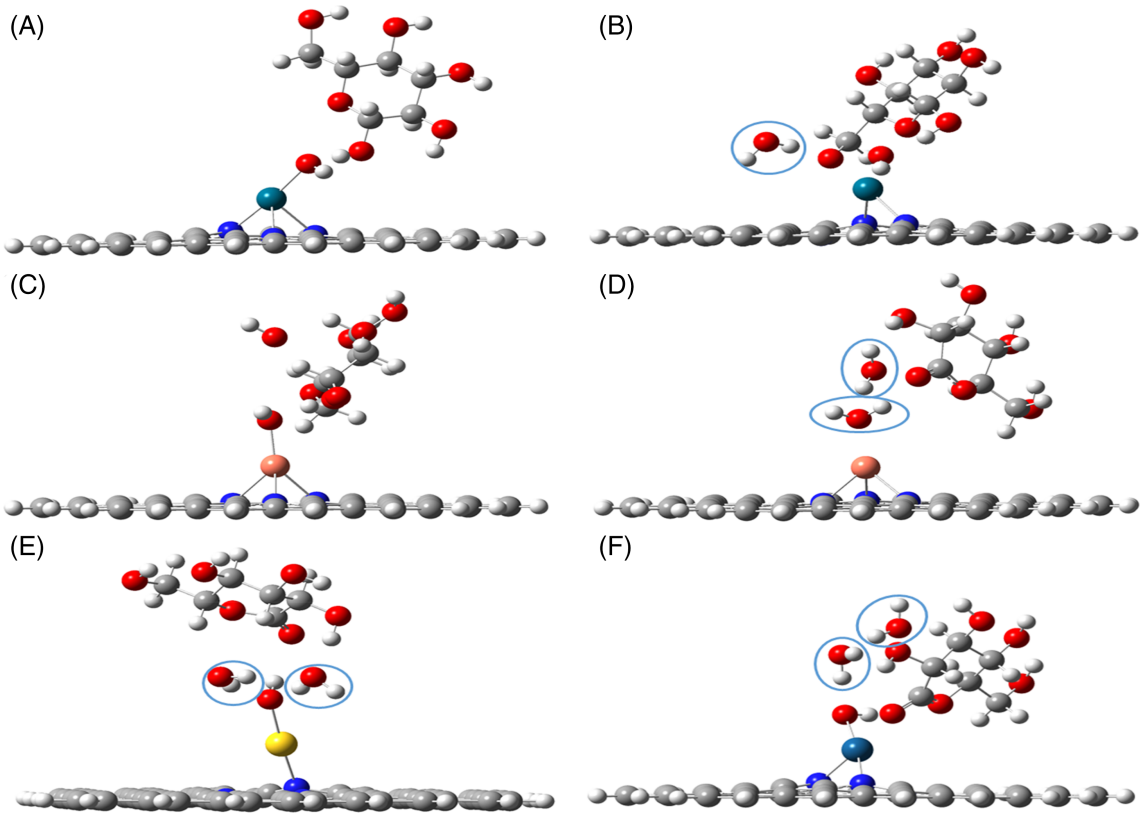

FIGURE 2 (A) Adsorbed $C_6H_{12}O_6$ molecule on the Pd-doped surface. (B) H_2O molecule and activated $C_6H_{11}O_6^-$ at site 5 on the Pd-doped surface. (C) Adsorbed $C_6H_{12}O_6$ molecule on the Cu-doped surface with electrolytic OH species placed at a distance of 1.50 Å. (D) Glucono-lactone and two H_2O molecules formed on the Cu-doped surface. (E) Products formed after reaction on the Au-doped surface. (F) Products formed after reaction on the Pt-doped surface (please refer to the Data S1 xyz data file for better visualization of the outputs)

site of the molecule is stronger than other sites. Our result is consistent with this explanation. In addition to the OH group, the calculation was performed to see the interaction strength of H atom of hemiacetal C because Ernst et al. stated that the oxidation reaction starts with H atom bonded to the hemiacetal C atom due to its strongly acidic OH-group.[76] However, approximately the same adsorption energy was obtained as −0.66 eV at a distance of 2.21 Å for this side. Pd-doped system was followed by the Cu-doped system with an adsorption energy of −0.49 eV. Although the energy released differed for Pd, Cu, and the others, the above-mentioned distances were the same for the whole system with one exception. The distance of the molecule to the surface OH species was 1.44 Å for Cu-3NG but 1.54 Å for other surfaces. Likewise, the most active site for the entire surface was obtained for the hemiacetalic OH site. No spontaneous water formation was observed after the interaction of $C_6H_{12}O_6$ with OH-surface species, but H atom seemed to be nearly split off from the glucose molecule. This event occurred in the same way for all doped atoms. The adsorption energy value of $C_6H_{12}O_6$ in various Au cluster systems was reported between −0.45 and −0.57 eV which is very close to the results we obtained.[70,71]

After stimulating the H atom of the hemiacetalic OH group, the second step of the oxidation reaction is the formation of water with OH species present in the electrolyte and H atom of $C_6H_{12}O_6$. Since the highest adsorption energy was obtained for Pd-doped surface, it was first investigated for the formation of H_2O for this catalytic system. Therefore, the OH-species in the electrolyte were located close to the stimulating H atom and hemiacetalic H. Although OH species were placed at various distances ranging from 1.0 and 1.6 Å, OH^- ion preferred to adsorb on the surface Pd atom instead of forming a water molecule. Before moving to other metal-doped surfaces, the interactions of the OH^- in the electrolyte solution with the sites 2–5 were examined. When OH species was put at site 2, it preferred adsorption on the graphene surface while a water molecule formed with the formation energy of −1.34 eV at site 3. OH groups away from the point where the molecule attaches to the surface, that is, site 4 and 5, tended to make water molecule with higher energy, −1.65 and −2.27 eV respectively. For site 5, the activated $C_6H_{11}O_6^-$ approached to the surface Pd atom through dehydrogenated O atom at $d_{Pd\text{-}C_6H_{11}O_6} = 2.07$ Å while forming a water molecule as shown in Figure 2B. Although high deprotonation energy was obtained for the site 5, the proposed gluconic acid mechanism does not follow this path. Instead of $C_6H_{11}O_6^-$, glucono-lactone must be formed first as an intermediate through the proposed mechanism. For this pathway, dehydration of $C_6H_{12}O_6$ molecule must proceed through the cleavage of the H atoms in the hemiacetal C region.

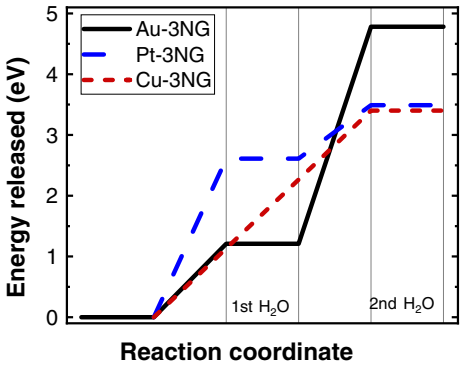

FIGURE 3 Energy release during the glucono-lactone formation on Au, Pt, and Cu doped 3NG surfaces

For the Cu-promoted surface, all sites of the $C_6H_{12}O_6$ molecule were again examined to reveal the behavior toward the OH species present in the electrolyte. When we put OH species near sites 4 and 5, the points where water formation occurred with high energy for Pd-3NG surface, water was formed again with −1.35 and −0.84 eV energy. Then the OH molecule was placed near the hemiacetalic H atom at a distance of 1.50 Å as shown in Figure 2C since it is reported as the most active point in the literature.[76] Contrary to the Pd-3NG surface, two water molecules were formed for this geometry with high exothermic energy of −3.45 eV. When the electrolytic OH species split the hemiacetal H atom from the $C_6H_{12}O_6$, the surface adsorbed OH species dissociated the H atom of the hemiacetal OH group. A single-step glucono-lactone formation occurred on the Cu-3NG electrode surface, and no adsorbed products or species present in the alkaline medium remained on the Cu atom at the end of the reaction as depicted in Figure 2D. Cu/CNT catalyst has been reported as one of the promising catalysts for energy production from glucose in direct alkaline FCs reactor in the experimental literature.[77]

The formation of glucono-lactone was investigated in different OH-species orientations on other metal surfaces (Pt, Au, Zn, Ni). Among various sites, the maximum deprotonation energy for the Au-3NG surface was obtained as −1.21 eV resulting in the cleavage of the hemiacetal H atom and the formation of the first H_2O molecule. By placing the second OH species next to the hemiacetal OH group at a distance of 1.50 Å, glucono-lactone and the second H_2O molecule were obtained with high exothermic energy of −4.78 eV. However, in the second step, electrolytic OH species did not directly remove H from the activated $C_6H_{11}O_6^-$ molecule; instead, it detached H from surface adsorbed OH, and the deprotonated surface O atom split H from the molecule. Water molecule formation took place for other sites of physically adsorbed $C_6H_{12}O_6$ molecule with energy less than −1.07 eV compared with the hemiacetal regions. Besides, in the hemiacetal OH site, electrolytic OH was adsorbed on the Au atom as a second molecule instead of H taken from the $C_6H_{12}O_6$ molecule. Glucono-lactone was formed on Au-3NG surface in a different pathway involving a two-step reaction with high exothermic energy. In the case of the Pt-3NG surface, OH species were placed at a distance of 1.50 Å from the hemiacetal H and OH regions. The OH species physisorbed on the hemiacetal H with an energy of −0.15 eV and the distance increased from 1.50 to 1.82 Å. On the other hand, a water molecule formed in the OH region by dissociation of H with significantly higher energy (−2.61 eV) and subsequent splitting of hemiacetal H atom resulted in the desired product. The second step released −3.49 eV of energy, which was smaller than that obtained for the Au-3NG surface. As shown in Figure 2E,F, unlike the Cu-3NG electrode, OH species remained on the metal atom after the completion of the reaction for both surfaces. The energy released on the surfaces where the glucono-lactone formation is visualized in Figure 3. Unlike the mechanism proposed by Ishimoto et al., OH species adsorbed on the surface or in the electrolytic medium did not bind to the deprotonated cyclic form of the glucose molecule. Instead, after the first H atom bond of the hemiacetal site was cleaved, the remaining second H atom was split off to form the glucono-lactone intermediate. The OH species present both on the electrode surface and in the electrolytic solution participated in this reaction. Glucono-lactone formation was not observed over Ni and Zn-doped surfaces as in the case of Pd-3NG electrode. The calculation results of various orientations showed that the maximum deprotonation energy released as −1.44 eV for Zn-doped surface and −1.46 eV for Ni-doped surfaces for site 2. Different from the Zn-3NG surface, the deprotonated O atom made a bond with a surface Ni atom. There was no interaction in the hemiacetal regions.

The identification of the intermediate during the electro-oxidation reaction was performed by in situ IR spectra and it was reported by Largeaud's group[35] that the band at 1728 cm^{-1} ascribed to the C═O vibration could be assigned to the C═O stretch of δ-lactone. This frequency value at 1728 cm^{-1} is shifted from the normal frequency value of 1740 cm^{-1} for the C═O vibration. The reason for this shift was interpreted as the adsorption of the molecule over the electrode surface. The IR frequency value attributed to lactone was checked for Cu, Au, and Pt-doped surfaces to evaluate the interaction of the product since the electro-oxidation reaction took place on these three surfaces in different pathways. The corresponding frequency values for lactone were calculated as 1687, 1725, and 1642 cm^{-1} for Cu, Au, and Pt-doped surfaces, respectively. When we look at the calculated values, the highest shift occurred for Pt-3NG surface because the distance between the molecule and the surface Pt atom was the smallest when compared with other surfaces. The measured distance for Pt and lactone was 2.13 Å. Moreover, it was 4.20 and 4.47 Å for Cu-3NG and Au-3NG surfaces, respectively. Therefore, from these results, it can be concluded that lactone is adsorbed physically over the Pt-3NG catalyst.

On the other hand, this interaction was very weak on the Cu-3NG surface, especially on the Au-3NG catalyst and the product desorbs spontaneously from the surface. When the results were evaluated with respect to their energy values as seen in Figure 3, it can be inferred that Au-doped graphene is the most effective catalyst in electro oxidation of the glucose molecule in the alkaline FC with a more exothermic reaction pathway. Besides, it can also be seen from the energy values that Cu and Pt catalysts are also promising catalysts with high exothermic reaction energy.

4 | CONCLUSIONS

In our DFT approach, the most examined metal atoms in GOR were used to model the SAC supported on the nitrogen-doped graphene surface to reveal the mechanisms that may occur during the reaction. The Au-3NG electrode which has a high electronegativity and small HOMO-LUMO band gap energy values adsorbed all ions in an alkaline medium more strongly. However, the adsorption of electrolytic OH species on the surface rearranged the electronic properties of the entire catalytic system and in this case, the Pd-doped 3NG electrode adsorbed $C_6H_{12}O_6$ molecule more strongly. Our computational results showed that glucono-lactone, which is reported as an intermediate in GOR, the formation took place over Cu, Pt, and Au-doped electrode surfaces and proceeded via different pathways. Direct formation of lactone occurred on Cu-3NG surface in a single-step reaction with an energy of −3.45 eV, and the metal surface remained empty after the reaction. On the other hand, the deprotonated $C_6H_{11}O_6^-$ molecule was first formed on the Pt and Au-doped electrode surfaces with −2.61 and −1.21 eV energies, respectively, and then the glucono-lactone formed with a second electrolytic OH species. The energy obtained for the second step was −3.49 eV for Pt-doped and −4.78 eV for Au-doped electrodes respectively. After a two-step reaction sequence, the adsorbed OH remained on the Pt and Au atoms. The vibrational frequency analyses consolidated the formation of the lactone with a small shift from the reported frequency value due to its adsorption on the surfaces. Although deprotonation of $C_6H_{12}O_6$ molecule on the Pd, Ni, and Zn-doped surfaces took place in the energy range of −1.44 to −2.27 eV, no lactone was formed. When the overall energy values and the intermediates formed during reaction are examined, it can be seen that single Cu, Pt, and especially Au-doped nitrogen decorated graphene surfaces are effective for direct glucose FC reactor in an alkaline medium.

ACKNOWLEDGMENTS

The density functional theory calculations reported in this paper were fully performed at TUBITAK ULAKBIM, High Performance and Grid Computing Center (TRUBA resources). Visit http://www.truba.gov.tr/ for more information.

DATA AVAILABILITY STATEMENT

The data that support the findings of this study are available from the corresponding author upon reasonable request.

ORCID

Derya Düzenli https://orcid.org/0000-0002-0057-8692
Ilker Tezsevin https://orcid.org/0000-0001-5648-3943

REFERENCES

[1] O. Z. Sharaf, M. F. Orhan, *Renew. Sustain. Energy Rev.* **2014**, *32*, 810.
[2] W. Wiyaratn, *Eng. J.* **2010**, *14*, 1.
[3] D. Akinyele, E. Olabode, A. Amole, *Inventions* **2020**, *5*, 42.
[4] S. Mekhilef, R. Saidur, A. Safari, *Renew. Sustain. Energy Rev.* **2012**, *16*, 981.
[5] A. Caglar, D. Düzenli, I. Onal, I. Tezsevin, O. Sahin, H. Kivrak, *Int. J. Hydrogen Energy* **2020**, *45*, 490.
[6] A. Caglar, D. Düzenli, I. Onal, I. Tezsevin, O. Sahin, H. Kivrak, *J. Phys. Chem. Solids* **2021**, *150*, 109684.
[7] B. C. Ong, S. K. Kamarudin, S. Basri, *Int. J. Hydrogen Energy* **2017**, *42*, 10142.
[8] L. An, R. Chen, *J. Power Sources* **2016**, *320*, 127.
[9] K. Tran, T. Q. Nguyen, A. M. Bartrom, A. Sadiki, J. L. Haan, *Fuel Cells* **2014**, *14*, 834.
[10] H. Xu, B. Yan, K. Zhang, J. Wang, S. Li, C. Wang, Y. Shiraishi, Y. Du, P. Yang, *Electrochim. Acta* **2017**, *245*, 227.
[11] A. Çağlar, A. Aldemir, H. Kivrak, *Fuller. Nanotub. Carbon Nanostruct.* **2018**, *26*, 863.
[12] J. N. Tiwari, R. N. Tiwari, G. Singh, K. S. Kim, *Nano Energy* **2013**, *2*, 553.
[13] L. Zeng, Z. K. Tang, T. S. Zhao, *Appl. Energy* **2014**, *115*, 405.
[14] J. Jiang, A. Wieckowski, *Electrochem. Commun.* **2012**, *18*, 41.
[15] T. Zhang, T. Asefa, *Adv. Mater.* **2019**, *31*, 1804394.
[16] J. Sanabria-Chinchilla, K. Asazawa, T. Sakamoto, K. Yamada, H. Tanaka, P. Strasser, *J. Am. Chem. Soc.* **2011**, *133*, 5425.
[17] Y. Wang, Y. Wan, D. Zhang, *Electrochem. Commun.* **2010**, *12*, 187.
[18] K. Dj. Popović, N.M. Marković, A.V. Tripković, and R.R. Adžić, *J. Electroanal. Chem. Interfacial Electrochem. 313*, 181 (**1991**).
[19] X. Yan, X. Ge, S. Cui, *Nanoscale Res. Lett.* **2011**, *6*, 313.
[20] D. Basu, S. Basu, *Int. J. Hydrogen Energy* **2012**, *37*, 4678.
[21] A. Brouzgou, L. L. Yan, S. Q. Song, P. Tsiakaras, *Appl. Catal. B* **2014**, *147*, 481.
[22] J. Chen, H. Zheng, J. Kang, F. Yang, Y. Cao, M. Xiang, *RSC Adv.* **2017**, *7*, 3035.
[23] G. Moggia, T. Kenis, N. Daems, T. Breugelmans, *ChemElectroChem* **2020**, *7*, 86.
[24] C. P. de León, F. C. Walsh, A. Rose, J. B. Lakeman, D. J. Browning, R. W. Reeve, *J. Power Sources* **2007**, *164*, 441.
[25] P. He, Y. Wang, X. Wang, F. Pei, H. Wang, L. Liu, L. Yi, *J. Power Sources* **2011**, *196*, 1042.
[26] H. D. Kıvrak, A. Caglar, T. A. Hansu, O. Sahin, *MANAS J. Eng.* **2020**, *8*, 1.
[27] G. Gnana kumar, G. Amala, S. M. Gowtham, *RSC Adv.* **2017**, *7*, 36949.
[28] K. Tian, M. Prestgard, A. Tiwari, *Mater. Sci. Eng., C* **2014**, *41*, 100.
[29] A. Brouzgou, P. Tsiakaras, *Top. Catal.* **2015**, *58*, 1311.
[30] M. Zhiani, A. Abedini, S. Majidi, *Electrocatalysis* **2018**, *9*, 735.
[31] D. Basu, S. Basu, *Electrochim. Acta* **2010**, *55*, 5775.
[32] B.-Y. Song, Y.-S. Li, Y.-L. He, Z.-D. Cheng, *Energy Proc.* **2014**, *61*, 2118.
[33] S. Kerzenmacher, J. Ducrée, R. Zengerle, F. von Stetten, *J. Power Sources* **2008**, *182*, 66.
[34] D. Basu, S. Basu, *J. Solid State Electrochem.* **2013**, *17*, 2927.
[35] N. Arjona, G. Trejo, J. Ledesma-García, L. G. Arriaga, M. Guerra-Balcázar, *RSC Adv.* **2016**, *6*, 15630.
[36] F. Largeaud, K. B. Kokoh, B. Beden, C. Lamy, *J. Electroanal. Chem.* **1995**, *397*, 261.
[37] J. K. Nørskov, J. Rossmeisl, A. Logadottir, L. Lindqvist, J. R. Kitchin, T. Bligaard, H. Jónsson, *J. Phys. Chem. B* **2004**, *108*, 17886.
[38] A. Chen, P. Holt-Hindle, *Chem. Rev.* **2010**, *110*, 3767.
[39] A. Kloke, F. von Stetten, R. Zengerle, S. Kerzenmacher, *Adv. Mater.* **2011**, *23*, 4976.
[40] E. Antolini, E. R. Gonzalez, *J. Power Sources* **2010**, *195*, 3431.
[41] D. R. Dekel, *J. Power Sources* **2018**, *375*, 158.
[42] Y.-J. Wang, J. Qiao, R. Baker, J. Zhang, *Chem. Soc. Rev.* **2013**, *42*, 5768.
[43] D. Chai, X. Zhang, S. H. Chan, G. Li, *J. Taiwan Inst. Chem. Eng.* **2019**, *95*, 139.
[44] S. Sultan, J. N. Tiwari, J.-H. Jang, A. M. Harzandi, F. Salehnia, S. J. Yoo, K. S. Kim, *Adv. Energy Mater.* **2018**, *8*, 1801002.

[45] B. Qiao, A. Wang, X. Yang, L. F. Allard, Z. Jiang, Y. Cui, J. Liu, J. Li, T. Zhang, *Nat. Chem.* **2011**, *3*, 634.
[46] N. Cheng, S. Stambula, D. Wang, M. N. Banis, J. Liu, A. Riese, B. Xiao, R. Li, T. K. Sham, L. M. Liu, G. A. Botton, X. Sun, *Nat. Commun.* **2016**, *7*, 13638.
[47] S. A. Wella, Y. Hamamoto, S. Suprijadi, Y. Morikawa, I. Hamada, *Nanoscale Adv.* **2019**, *1*, 1165.
[48] X. Zhang, S. Zhang, Y. Yang, L. Wang, Z. Mu, H. Zhu, X. Zhu, H. Xing, H. Xia, B. Huang, J. Li, S. Guo, E. Wang, *Adv. Mater.* **2020**, *32*, 1906905.
[49] L. Zhou, P. Zhou, Y. Zhang, B. Liu, P. Gao, S. Guo, *J. Energy Chem.* **2021**, *55*, 355.
[50] Z. Feng, Z. Yang, X. Meng, F. Li, Z. Guo, S. Zheng, G. Su, Y. Ma, Y. Tang, X. Dai, *J. Mater. Chem. A* **2022**, *10*, 4731.
[51] Y. Tang, W. Chen, H. Chai, G. Zhao, Y. Li, D. Ma, X. Dai, *J. Phys. Chem. C* **2019**, *123*, 10926.
[52] S. Sultan, J. N. Tiwari, A. N. Singh, S. Zhumagali, M. Ha, C. W. Myung, P. Thangavel, K. S. Kim, *Adv. Energy Mater.* **2019**, *9*, 1900624.
[53] M. N. Groves, C. Malardier-Jugroot, M. Jugroot, *J. Phys. Chem. C* **2012**, *116*, 10548.
[54] C. Rivera-Cárcamo, P. Serp, *ChemCatChem* **2018**, *10*, 5058.
[55] Z. Liu, T. He, K. Liu, W. Chen, Y. Tang, *RSC Adv.* **2017**, *7*, 7920.
[56] M. Ha, D. Y. Kim, M. Umer, V. Gladkikh, C. W. Myung, K. S. Kim, *Energy Environ. Sci.* **2021**, *14*, 3455.
[57] Y. Tang, W. Chen, J. Shi, Z. Wang, Y. Cui, D. Teng, Y. Li, Z. Feng, X. Dai, *J. Mater. Chem. A* **2021**, *9*, 15329.
[58] Y. Tang, W. Chen, B. Wu, G. Zhao, Z. Liu, Y. Li, X. Dai, *ChemPhysChem* **2019**, *20*, 2506.
[59] Y. Tang, H. Zhang, W. Chen, Z. Li, Z. Liu, D. Teng, X. Dai, *Appl. Surf. Sci.* **2020**, *508*, 145245.
[60] J. Wu, L. Ma, R. M. Yadav, Y. Yang, X. Zhang, R. Vajtai, J. Lou, P. M. Ajayan, *ACS Appl. Mater. Interfaces* **2015**, *7*, 14763.
[61] J. Lee, S. Kwon, S. Kwon, M. Cho, K. Kim, T. Han, S. Lee, *Nanomaterials* **2019**, *9*, 268.
[62] C. Lee, W. Yang, R. G. Parr, *Phys. Rev. B* **1988**, *37*, 785.
[63] A. D. Becke, *Phys. Rev. A* **1988**, *38*, 3098.
[64] J. Baker, M. Muir, J. Andzelm, A. Scheiner, *ACS Symposium Series*, **1996**, *629*, 342.
[65] Gaussian 09, Revision A.02. Gaussian Inc.,Wallingford, CT, **2009**.
[66] M. W. Wong, *Chem. Phys. Lett.* **1996**, *256*, 391.
[67] M. F. Fellah, *Appl. Surf. Sci.* **2017**, *405*, 395.
[68] M. F. Fellah, *Int. J. Hydrogen Energy* **2019**, *44*, 27010.
[69] R. A. van Santen, *Modern Heterogeneous Catalysis*, Wiley-VCH Verlag GmbH & Co. KGaA, Weinheim, Germany **2017**.
[70] T. Ishimoto, H. Kazuno, T. Kishida, M. Koyama, *Solid State Ionics* **2014**, *262*, 328.
[71] T. Ishimoto, Y. Hamatake, H. Kazuno, T. Kishida, M. Koyama, *Appl. Surf. Sci.* **2015**, *324*, 76.
[72] A. M. Shendurse, C. D. Khedkar, *Encyclopedia of Food and Health*, Elsevier, **2016**, p. 239. https://doi.org/10.1016/B978-0-12-384947-2.00353-6
[73] S. Ramachandran, P. Fontanille, A. Pandey, C. Larroche, *Food Technol. Biotechnol.* **2006**, *44*, 185.
[74] M. Malček, S. Müllerová, L. Bučinský, *Physica E Low-Dimens. Syst. Nanostruct.* **2022**, *139*, 115144.
[75] R. L. Doyle, M. E. G. Lyons, *J. Solid State Electrochem.* **2014**, *18*, 3271.
[76] S. Ernst, J. Heitbaum, C. H. Hamann, *Ber. Bunsenges. Phys. Chem.* **1980**, *84*, 50.
[77] O. F. Er, H. Kivrak, *Energy Storage* **2021**, *3*, e271.

SUPPORTING INFORMATION

Additional supporting information can be found online in the Supporting Information section at the end of this article.

How to cite this article: D. Düzenli, I. Onal, I. Tezsevin, *J. Comput. Chem.* **2022**, *43*(26), 1793. https://doi.org/10.1002/jcc.26981